



**HAL**  
open science

## Multiscale characterization of hierarchically organized porous hybrid materials

Adeline Hardy-Dessources, Sarah Hartmann, Mohamed Baba, Nicola Huesing,  
Jean-Marie Nedelec

► **To cite this version:**

Adeline Hardy-Dessources, Sarah Hartmann, Mohamed Baba, Nicola Huesing, Jean-Marie Nedelec. Multiscale characterization of hierarchically organized porous hybrid materials. *Journal of Materials Chemistry*, 2012, 22 (6), pp.2713-2720. 10.1039/c1jm14905a . hal-00673064

**HAL Id: hal-00673064**

**<https://hal.science/hal-00673064v1>**

Submitted on 22 Feb 2012

**HAL** is a multi-disciplinary open access archive for the deposit and dissemination of scientific research documents, whether they are published or not. The documents may come from teaching and research institutions in France or abroad, or from public or private research centers.

L'archive ouverte pluridisciplinaire **HAL**, est destinée au dépôt et à la diffusion de documents scientifiques de niveau recherche, publiés ou non, émanant des établissements d'enseignement et de recherche français ou étrangers, des laboratoires publics ou privés.

# Multiscale characterization of hierarchically organized porous hybrid materials

*A. Hardy Dessources<sup>1,2</sup>, S. Hartmann<sup>3</sup>, M. Baba<sup>4,5</sup>, N. Huesing<sup>6</sup> and*

*J.M. Nedelec<sup>\*1,2</sup>*

1 Clermont Université, ENSCCF, Laboratoire des Matériaux Inorganiques, BP 10448,  
F-63000 Clermont-Ferrand, France

2 CNRS, UMR 6002, LMI, F-63177 Aubière

3 C2P2-Laboratoire de Chimie OrganoMétallique de Surface, CPE-Lyon, BP 2077,  
F-69616 VILLEURBANNE, France

4 Clermont Université, Université Blaise Pascal, LPMM, BP 10448,  
F-63000 CLERMONT-FERRAND, France

5 CNRS, UMR 6505, LPMM, F-63177 Aubière

6 Materials Chemistry, Paris-Lodron University Salzburg, Hellbrunner Str. 34, A-5020 Salzburg,  
Austria

---

\* Pr J.M. Nedelec, Bâtiment Chimie 7, Laboratoire des Matériaux Inorganiques, CNRS UMR 6002, 24 Avenue des Landais, 63177 Aubière Cedex, France  
+ 33 4 73 40 71 95  
j-marie.nedelec@univ-bpclermont.fr

## **Abstract**

In this work, monolithic hybrid materials exhibiting both meso- and macropores of controlled size have been prepared using the hydrolysis-condensation of modified silicon alkoxide in the presence of a surfactant. These materials have been thoroughly characterized using gas sorption, mercury intrusion porosimetry, small angle X-ray scattering and electronic microscopies both in scanning and transmission modes. Using these hierarchically porous samples, it has been possible to demonstrate for the very first time that thermoporosimetry (TPM) technique, based on the measurement of transitions of confined liquids, is indeed valid over a very wide pore size range (from few nm up to several hundred nm) to characterize the porosity in solids. This first experimental evidence is a major breakthrough because it offers a unique technique covering the whole range from mesopores to macropores, filling the known gap from standard techniques. This unique combination of smart design of hierarchically porous materials and advanced calorimetric characterization of porous solids, has also brought the first true calibration data for TPM on such a large size scale.

## **Introduction**

Nature has always been a source of inspiration for chemists and materials scientists. Among the most striking features of natural materials, the 3-dimensional organization of matter at different length scales has attracted considerable interest during the last 20 years. The so-called hierarchical materials are found in many natural systems such as bone tissue, wood, nacre, or diatoms and are becoming a major source of inspiration for material scientists<sup>[1]</sup>. Especially the siliceous exoskeleton of diatoms provides a magnificent example of an organized hierarchical system occurring in a living organism in which the beauty of a highly periodically ordered pore system and the functionality – the mass transfer within the organism- are combined.<sup>[2]</sup>

For a wide variety of applications, such as catalytic reactors,<sup>[3,4,5]</sup> sorption or separation sciences,<sup>[6,7]</sup> biomaterials engineering, or as scaffolds, simple and efficient methods are needed to produce materials comprising several level of pore sizes, e.g. macro/meso or macro/micro in diverse morphologies. This is especially true for applications, which rely on the contact of the solid phase with a fluid. A highly interconnected or co-continuous

macroporous framework allows for a high diffusion rate at low pressure drop through the solid material, whereas the meso/ micropore system guarantees for a high internal specific surface area and thus for a high loading with reactive sites.

In recent years several approaches have been developed to deliberately design meso/macroporous silica-based monoliths, e.g. relying on templating methods, or phase separation strategies. To name only some recent examples, Nakanishi has pioneered the phase separation strategy by relying on spinodal decomposition of polymers in a silica sol-gel system<sup>[8]</sup> and Hüsing et al. followed a similar strategy and highly porous silica monoliths with a cellular macroporous network comprising hexagonally arranged mesopores were obtained.<sup>[9]</sup>

Concomitantly with the development of designing hierarchically organized materials across varying length scales<sup>[10,11,12]</sup>, a key issue is to find efficient characterization techniques in order to investigate and determine the different pore size regimes.

Several techniques have consequently been developed to characterize the structure of porous solids. Among them, gas sorption and mercury intrusion porosimetry are probably the most popular. Gas sorption is very efficient for microporous and mesoporous solids with reasonably small pore size (few tenth of nm in diameter) resulting in an observable capillary condensation described by the Kelvin equation. The latter allows for the correct determination of pore size distribution assuming a given pore shape. On the other end of the scale, mercury intrusion porosimetry is well adapted for large macropores for which the intrusion of non-wetting mercury occurs at reasonably low pressure. This pressure is related to the size of the pores through the well known Laplace-Washburn equation. When the pores are getting smaller, the intrusion pressure increases strongly and reaches considerable values for mesopores rendering the technique questionable because of the most probable alteration of the pore structure, sometimes even leading to the destruction of the material. Consequently a gap covering the range of large mesopores up to small macropores exists where no single technique is available with good confidence.

Alternative techniques relying on the Gibbs-Thomson equation <sup>[13,14]</sup> have also been proposed. This equation quantifies the observed experimental shift of the melting point of a liquid confined in pores and can be written:

$$\Delta T = T_p - T_0 = \frac{2\sigma_{SL} \cos \theta T_0}{\Delta H_m \rho_s R_p} \approx \frac{k}{R_p} \quad \text{Equation (1)}$$

where  $T_p$  is the melting temperature of a liquid confined in a pore of radius  $R_p$ ,  $T_0$  is the normal melting temperature of the liquid,  $\sigma_{SL}$  is the surface energy of the solid/liquid interface,  $\theta$  the contact angle,  $\Delta H_m$  is the melting enthalpy and  $\rho_s$  the density of the solid.

According to this equation, the shift of the transition temperature of a confined liquid  $\Delta T$  is inversely proportional to the radius of the pore in which it is confined. In fact it is well known that not all the solvent takes part in the transition and that a significant part of it remains adsorbed on the surface of the pore. The state of this adsorbed layer has been discussed extensively in the case of water. Consequently, the radius measured by application of the Gibbs-Thomson equation should be written  $R=R_p-t$  where  $t$  is the thickness of the adsorbed layer leading to a reformulation<sup>[15]</sup> of Equation 1 as

$$R_p = \frac{k}{\Delta T} + t \quad \text{Equation (2)}$$

In principle, it is then possible to determine the pore size of a given material by measuring  $\Delta T$ . In 1955 Kuhn et al.<sup>[16]</sup> proposed to use Differential Scanning Calorimetry to measure  $\Delta T$  and invented the so called thermoporometry technique (or thermoporosimetry as will be used in the following). This technique has been further described by Fagerlund<sup>[17]</sup> and popularized and developed by Brun<sup>[18]</sup>. Knowledge of  $k$  and  $t$  in Equation 2 is mandatory, but once determined, the curve obtained from thermoporosimetry (TPM) can be transformed into the pore size distribution. In this sense, TPM is a secondary method since it requires preliminary determination of the evolution of  $\Delta T$  as a function of  $R_p$  for a given solvent.

It has been shown<sup>[19]</sup> that the correlation between gas sorption and TPM is good making the later an interesting alternative for measuring pore size distribution.

Among the many advantages of TPM, the authors have been exploring thoroughly two applications in the recent years.

First, TPM is also applicable to soft materials like polymers and gels where the characterization of mesh size distribution is possible together with the determination of swelling ratio<sup>[20,21]</sup> and even dynamics including the measurement of diffusion coefficients in confined geometry<sup>[22]</sup>. Of particular interest is the study of aging in polymers<sup>[23]</sup> and nanocomposites made up of interpenetrating organic and inorganic networks<sup>[24]</sup>.

Secondly, the range of applicability of TPM is expected to be much larger than gas sorption and indeed many applications of TPM on the macro scale (beyond 50 nm) can be found now in the literature including hierarchically porous TiO<sub>2</sub> microparticles<sup>[25]</sup>. The only limitation is the lack of confident calibration of TPM in the macropore domain. Indeed since the early developments, mesoporous solids have always been used for calibration purpose with a limited demonstrated validity<sup>[26,27]</sup>. All derivation of TPM on bigger pore sizes, are somehow speculative even if comparative studies and comparison with SEM are all conclusive.

The goal of this work is to report the first true calibration of TPM in the macropore domain together with mesopores, thus confirming the long time established hypothesis that TPM can indeed be used as a multiscale characterization technique for porosity in solids and 3D network organization in soft materials. This makes TPM very unique and confirms it as the missing element in the full size range characterization set of techniques.

To achieve this objective, hierarchically porous hybrid materials have been prepared by using an ethylene glycol modified silane (EGMS) as precursor. These materials exhibit both mesopores and macropores, the size of which can be tuned by carefully selecting the structure-directing and phase-separation inducing agent, here Pluronic P123, and via controlling hydrolysis and condensation reactions by adjusting the concentration of the acidic catalyst HCl. The porosity of these materials has been completely characterized by gas sorption and mercury porosimetry allowing to confirm the validity of TPM on both size ranges and to derive the first true multiscale calibration of TPM with o-xylene.

## Experimental section

### *Chemicals and solvents*

Ethylene glycol (>99.5 %, Merck) was first dried over Na<sub>2</sub>SO<sub>4</sub> and then purified by distillation over magnesium. Tetraethoxysilane (>99.0 %, Merck) was employed as purchased. As surfactant and phase separation agent poly(ethylene glycol)-block-poly(propylene glycol)-block-poly(ethylene glycol) (Pluronic P123<sup>TM</sup>, M<sub>n,av</sub> = 5800 g·mol<sup>-1</sup>), EO<sub>20</sub>PO<sub>70</sub>EO<sub>20</sub> (Aldrich) was used without further purification. Hydrochloric acid (32 %, NORMAPUR, VWR BDH Prolabo) was employed as acid catalyst for hydrolysis and condensation reactions. The solvents ethanol, petroleum ether (VWR BDH Prolabo) and the silylating agent chlorotrimethylsilane (>99.0 %, Merck) were applied as purchased. For thermoporosimetry measurements, HPLC grade o-xylene (Aldrich) was used without further purification.

### *Synthesis of the glycolated precursor*

The ethylene glycol modified silane (EGMS) was synthesized via a transalkoxylation reaction by reacting tetraethoxysilane with ethylene glycol in a molar ratio of 1:4 in argon atmosphere at 413 K<sup>[28]</sup>. During the synthesis ethanol was continuously removed by distillation. When no more progress of the reaction could be observed, excess of ethanol and tetraethoxysilane were removed in *vacuo* and the resulting SiO<sub>2</sub>-content of the liquid product was determined by thermogravimetric analysis (TGA). The here employed EGMS contained 20.6 wt% SiO<sub>2</sub> (theoretically expected value for SiO<sub>2</sub>: 22 wt%). The purity of EGMS was determined by spin-lock <sup>29</sup>Si-NMR investigations and showed one peak at -81.86 ppm indicative of the Si species with four glycolate ligands and at -88.60 ppm which can be assigned to either bridged-Si species or chelated Si species resulting either of intermolecular or intramolecular condensation reactions<sup>29</sup>.

### *Monolith Preparation*

Three wet gels (A, B, C) were prepared by adding a homogeneous mixture of Pluronic P123<sup>TM</sup> and dilute hydrochloric acid to EGMS whereas the concentration of the acid was either 1, 0.1 or 0.03 mol/l for A, B and C, respectively. The composition (by mass) of Si : P123 : x M HCl was adjusted to 8.4 : 30 : 70, assuming complete conversion of EGMS to silica<sup>[29]</sup>.

After homogenization of the mixture (using a vortex stirrer) the sol was allowed to gel and age in cylindrical PE vessels at 313 K for 7 days.

After aging all gels were cured for 6 h in a mixture of ethanol and concentrated hydrochloric acid (50 : 50 vol%), resulting in a higher mechanical strength. To avoid cracking of the monoliths during drying, all samples were treated by silylation of the surface silanol moieties with trimethylchlorosilane in petroleum ether (10 : 90 vol%), followed by washing with petroleum ether and ethanol to eliminate unreacted silane species<sup>[30]</sup>.

At last all samples were slowly heated to 473 K to remove residual solvent and simultaneously preserving the methyl moieties on the silica surface, resulting in a hydrophobic surface of the silica network.

### Characterization

The spin-lock  $^{29}\text{Si}$ -NMR investigations of the glycol modified silane were performed on a Bruker Digital NMR AV 400 spectrometer (Bruker, Karlsruhe) at 79.5 MHz in benzene- $d_6$  as solvent. For the spin-lock method (WALTZ16)<sup>[31,32]</sup>, a 90° pulse of 50  $\mu\text{s}$  was applied for  $^1\text{H}$  and  $^{29}\text{Si}$  nuclei attenuating of 16 dB and 11 dB, respectively. Nitrogen sorption measurements were performed on a NOVA 4000e instrument (Quantachrome Instruments, Boynton Beach, FL) at 77 K in the relative pressure range of  $p/p_0 = 0.05 - 0.99$ . All samples were degassed for 3 h at 373 K *in vacuo* prior to analysis. The BET surface area was determined using the 5 point method in a relative pressure range from 0.05 – 0.3. The mesopore size distribution was calculated on the basis of the desorption branch using the BJH model.<sup>[33,34]</sup>

Small angle X-ray scattering (SAXS) measurements were performed on a Nano-STAR instrument (Bruker AXS, Karlsruhe) equipped with a HI-STAR area detector (Bruker AXS, Karlsruhe). The X-ray radiation was generated by a Cu anode ( $\lambda_{\text{K}\alpha} = 0.154 \text{ nm}$ ) and the distance between sample and detector was 106 cm from which scattering curves in the range of  $0.2 - 2.1 \text{ nm}^{-1}$  were obtained. All SAXS patterns were radially averaged to achieve the function  $I(q)$  with the scattering vector  $q = (4\pi\sin\theta/\lambda)$  ( $2\theta =$  diffraction angle,  $\lambda = 0.154 \text{ nm}$ ). All values were corrected for background scattering from the experimental setup.

The size distributions of the macropores were determined by mercury intrusion measurements on a Porosimeter 2000 (Fisons Instruments) in the pressure range from ambient pressure up to 2000 bar. The pore size distribution was calculated by applying the Washburn equation  $R = (-2\gamma\cos\theta/p)$  for a cylindrical pore geometry (mercury: contact angle  $\theta = 140^\circ$  (at 20°C), surface tension  $\gamma = 480 \text{ mN/m}$  (at 20°C)).

The porous morphology of the silica gels was either investigated by scanning electron microscopy (SEM) with a Zeiss DSM-962 instrument (Carl Zeiss AG, Jena) ( $U = 10 \text{ kV}$ ) after sputtering with Au-Pd (thickness of layer: 20 nm) to visualize the macroporous network or by transmission electron microscopy (TEM) with a Philips 400 ( $U = 80 \text{ kV}$ ) on copper grids.

For thermoporosimetry measurements, *ortho*-xylene was chosen as a probe solvent for its good wettability of the hydrophobic surfaces resulting from the silylation procedure. TPM analyses were performed by differential scanning calorimetry (DSC) measurement with a Mettler-Toledo DSC 823<sup>e</sup> apparatus, using STAR<sup>e</sup> software. The DSC apparatus was calibrated (both for temperature and enthalpy) with metallic standards (In, Pb) and n-heptane. About



30 to 40 mg of the soaked sample was introduced into an aluminium DSC pan of 160  $\mu\text{l}$  with an excess of *o*-xylene. The measurement procedure under air atmosphere included the following steps: Cooling from  $-10^{\circ}\text{C}$  to  $-90^{\circ}\text{C}$  at a rate of  $10^{\circ}\text{C}/\text{min}$ ; heating from  $-90^{\circ}\text{C}$  to  $-28^{\circ}\text{C}$  at a rate of  $0.7^{\circ}\text{C}/\text{min}$ ; and a last cooling from  $-28^{\circ}\text{C}$  to  $-90^{\circ}\text{C}$  at a rate of  $0.7^{\circ}\text{C}/\text{min}$ . A slow rate of  $0.7^{\circ}\text{C}/\text{min}$  was chosen to allow the continuous thermal equilibrium inside the DSC cell.

## Results and discussion

### Porosity and morphology

Monolithic samples are very convenient, both for practical applications such as stationary phases for chromatography but also in our case due to easy shaping and handling of the samples (Figure 1). Three samples were prepared by varying the employed HCl concentration from 1 to  $0.03 \text{ mol L}^{-1}$ . All samples exhibit a co-continuous macroporosity as evidenced by SEM, with a distinct influence of the hydrochloric acid concentration on the resulting macroporous network (see Figure 2; the scale bar is  $5 \mu\text{m}$  for all images). The variation in the concentration of the acid catalyst, thus the pH-value of the initial mixtures, provides an efficient way to tune the macropore size which is highly desirable for TPM calibration. The monolith prepared with  $1 \text{ mol}\cdot\text{L}^{-1}$  HCl shows a quite narrow pore radii distribution with a maximum of about 140 nm as determined by mercury intrusion measurements. Employing lower concentrations of HCl *e.g.*  $0.1 \text{ mol}\cdot\text{L}^{-1}$  HCl, results in a more coarsened co-continuous macroporous network with pore radii of 240 nm, whereas a further dilution of the acid to  $0.03 \text{ mol}\cdot\text{L}^{-1}$  HCl decreases the average radius of the macropores again to about 190 nm.

This behaviour can be explained by the strong dependence of the pH-value on hydrolysis and condensation rates resulting in a different timing of the phase separation and gelation process. The latter one freezes the momentary situation of the phase separated domains and therefore determines the final macroporous morphology including the pore sizes. TEM images clearly show that the samples are not only mesoporous with pore diameters in the range of about 6 nm, but that the pores are in addition highly monodisperse and exhibit a long range ordering of a 2D-hexagonal arrangement as expected from the templating with P123 (as an example Sample A is displayed in Figure 3).<sup>[35]</sup> From scanning electron

microscopy it is quite clear that the samples exhibit both, meso- and macropores, with the size of the macropores being strongly dependent on the concentration of hydrochloric acid (pH value).

For a more quantitative investigation of the mesopore size and the arrangement, all samples have been subjected to SAXS analysis and results can be found in Figure 4. The patterns are very similar for the three samples, thus confirming that the influence of the pH-value in this size regime is only of minor importance. In addition, the 2D-hexagonal packing of the mesopores with a repeating unit distance of  $d_{10} = 11.2$  nm for the monolith prepared with 0.03 M HCl up to  $d_{10} = 11.6$  nm for the sample synthesized from 0.1 M is clearly evidenced (main reflections are assigned in the figure) with the expected sequence of reflections of  $1 : \sqrt{3} : 2$ . The lattice constant  $a$  for the hexagonal lattice can be calculated to 13 nm. However, the relative intensities of the reflections – especially for the (11) and (20) reflections - show minor differences to each other for the various pH-values, which can be attributed to the different form factors arising from differences in the respective pore wall thicknesses and pore diameters. This has already been discussed previously.<sup>[36,37]</sup>

### **Gas sorption analysis**

The three samples have been characterized in more detail with respect to their porous structure by nitrogen sorption analysis at 77 K. All samples show similar isotherms. Representative isotherm of sample A is shown in Figure 5 exhibiting a type IV isotherm hysteresis loop all typical of mesoporous solids. Specific surface area and mean mesopore size have been determined with the classical models, BET and BJH, respectively. The applicability of the BJH model is supported by the observed cylindrical nature of the mesopores (Figure 3). All data are collected in Table 1.

As can be seen from the pattern of the nitrogen sorption hysteresis and the scattering pattern in figure 4, the changes of the concentration of the acid catalyst in the range from 1 to 0.03 mol L<sup>-1</sup> have no great impact on the formation of the 2D-hexagonally organized mesopore system.

### **Mercury porosimetry**

On the other hand, the macroporous morphology seems to be greatly influenced by the concentration of HCl acid as depicted in Figure 2. Dependent on the timing of the phase-

separation into a silica-rich phase as well as solvent-rich phase and the sol-gel transition – thus the solidification of the network – , the resulting macroporous morphology is determined. However, due to Ostwald-ripening and syneresis effects altering of the gelled silica network occurs until a complete solidification of the phase-separated domains, resulting in a finer macroporous framework for early solidified phase-separated systems or for a later solidification in a more coarsened macroporous network vice versa.

Mercury intrusion porosimetry has thus been used for the determination of a mean macropore size. As can be evidenced from Figure 2, the macropore size distribution looks also quite narrow. The values obtained are presented in Table 1 together with gas sorption data. An important deviation of baseline in mercury intrusion curves rendered the determination of macroporous volume impossible.

These fully characterized samples can now be used as calibration materials for TPM.

### **Thermoporosimetry**

TPM has been performed on all samples with o-xylene as a probe solvent. Visual wetting of the samples by the solvent was confirmed and the o-xylene was added in slight excess in order to be sure to both completely fill the porosity and to have some free solvent allowing the measurement of its crystallization. As usually performed with this solvent, crystallization curves have been used instead of melting but reversibility of the transitions has been checked upon cycling the system. The thermogram obtained for sample A is shown in Figure 6. Three crystallization peaks are observed for o-xylene in this system. The first one close to -26 °C corresponds to free solvent. Close to this peak a second one is observed and attributed to macropores. Finally a third peak highly shifted towards low temperatures is observed around -70 °C and corresponds to a strong degree of confinement and thus to mesopores. It is clear from Figure 6 that both mesopores and macropores contribution can be extracted from the thermogram. The proximity and partial convolution of the free solvent peak and the macropore peak requires deconvolution procedure that has been performed using gaussian functions and least square refinement. For this reason, quantitative information (macroporous volume and macropore size distribution) could not be obtained because the solvent confined in macropores was not completely melted resulting in underestimation.

O-xylene calibration with mesoporous silica gels (pore radius ranging from 2.4 nm to 14.3 nm) has been reported earlier by the authors<sup>38</sup> and the following equation was derived:

$$R_p = t \exp\left(\frac{-1}{c\Delta T}\right) \quad \text{Equation (3)}$$

with  $t = 1.814$  nm being the thickness of the layer of the solvent remaining adsorbed on the surface of the pores, and  $c = 0.03842$  °C<sup>-1</sup>.

This mathematical model is different from equation 2 but avoids inherent simplification hypothesis and has proven to be the most suitable for this solvent in particular for the high value of  $R_p$ <sup>39</sup>.

As critically discussed<sup>18</sup>, in order to correctly derive the pore size distribution, one has to take into account the variation of the enthalpy of crystallization of the solvent as a function of temperature. This was also done by considering the amount of o-xylene undergoing the transition knowing the porous volume of the reference silica gels.

Following dependence was found:

$$W_a = W_o \exp\left(\frac{\Delta T}{f}\right) \quad \text{Equation (4)}$$

with  $W_o = 97.7$  J.cm<sup>-3</sup> the energy of crystallisation of the bulk solvent and  $f = 57.9$  °C.

Considering both equations (3) and (4) derived for mesoporous systems, pore size distributions (PSD) can be determined following :

$$\frac{dV_p}{dR_p} = \frac{Y(T) \cdot \Delta T^2 \cdot c}{W_a \cdot R_p} \quad \text{Equation (5)}$$

with  $Y(T)$  the signal from the DSC.

The PSD have been calculated for mesopores for all samples by transforming the thermograms according to equation (5). The calculation for macropores was not possible because of the proximity of the two peaks in the DSC curve.

For mesopores, the comparison of TPM derived and gas sorption derived PSDs is good as illustrated with the example of sample A (Figure 7). The most probable pore sizes derived from TPM are compared to the values obtained by nitrogen sorption in Table 1. The

incertitude for TPM measurements have been estimated, they come mainly from the TPM calibration curve. Data presented in this paper demonstrate incertitude ranging from 2 to 9 % for macropores and less than 5% for mesopores. It is worthy to note that this incertitude is calculated with other techniques (gas sorption or mercury intrusion) as a reference considering that it gives the exact value. Indeed these techniques have also their own incertitude so that the incertitude estimated here is maximized.

Calibration being obtained with mesoporous samples, the excellent correlation (discrepancy being within the experimental error) shown in Table 2 is nice but not surprising. It nevertheless validates the use of TPM on these new hybrid samples confirming also that TPM is not affecting the mesopores upon measurement contrary to Hg porosimetry.

Concerning the macropores, deconvoluted macropore peaks are shown in Figure 8. The most probable macropore size (taken at the maximum of the peak) have been determined using equation (3). Values are given on the Figure and also reported in Table 2. The correlation with Hg-porosimetry data is good and in particular the non monotonous evolution as a function of HCl concentration (B>C>A) is reproduced. To check the good predictive value of the calibration curve derived with mesoporous samples only, all data are gathered in Figure 9. In this figure, squares symbols represent the reference silica gels used for obtaining calibration Equations (3) and (4). The circles correspond to the mesopores of samples A, B and C and triangles to macropores of the same samples. All those values correspond to the pore size as determined by gas sorption and Hg porosimetry. The dotted line representing equation 3 exhibit a very good predictive character as all points fall very close to the line. In particular it is striking to observe that over more than three decades (from 1 to 300 nm) the calibration curve obtained with mesoporous samples only is completely valid. This obviously confirms the applicability of TPM in the macropore domain and that calibration curves obtained on mesoporous samples and published in the literature can be applied safely on longer length scales.

Furthermore, because the values of the macropores are known from Hg porosimetry, it is possible to refine the calibration curve a bit more. In this sense Orthogonal Distance Regression (ODR) minimizing for each point the distance between the fitting curve and the experimental points has been performed on the data yielding the following definitive calibration curve for o-xylene over the whole range of size:

$$R_p = 1.4919 \exp\left(\frac{-1}{0.03706 \Delta T}\right) \quad \text{Equation (6)}$$

This curve is also drawn in Figure 9 as a continuous line. Clearly the deviation from Equation (3) is small but this consists in the first ever reported calibration curve for TPM including both mesopores and macropores opening a wide range of applications to more complex materials exhibiting for instance hierarchical porosity.

## Conclusions

For the first time, the validity of TPM beyond the mesopores domain has been demonstrated. Using modified silicon alkoxide, hierarchically porous hybrid materials have been prepared. By changing the synthesis conditions, the macropore size was tuned allowing the use of these materials as reference for TPM. Classical techniques have been used to fully characterize the porosity of the materials, gas sorption, SAXS and TEM for mesopores and mercury intrusion porosimetry and SEM for macropores. TPM gives a very good prediction of both meso and macropores sizes validating its use with other solvents. Furthermore, it has been possible to refine the calibration curve for o-xylene over the whole pore size range from 1 to 300 nm, which is the first known example in the literature. This opens the way towards the multiscale characterization of complex systems including polymers, hybrid and nanocomposites just to cite a few. The possibility of using various and sometimes complex liquid probes for TPM makes this technique attractive to the whole chemistry of materials community as exemplified in our recent work<sup>[24,25,38]</sup>.

## Acknowledgements

The Conseil Régional de la Martinique is acknowledged for funding.

## Figures and Tables captions

Figure 1: Picture of a monolithic hybrid sample.

Figure 2: SEM pictures of samples A, B, C (same scale) showing open interconnected macropores.

Figure 3: TEM image of sample A showing mesopores of cylindrical nature (on the left) with regular 2D hexagonal packing (bottom right).

Figure 4: SAXS patterns from samples A, B and C with main reflections assignment.

Figure 5: Typical nitrogen gas sorption isotherm of sample B.

Figure 6: DSC thermogram obtained on sample A filled with o-xylene upon cooling from room temperature.

Figure 7: Mesopore size distribution obtained by TPM (line) and nitrogen desorption (-○-) on sample A, mean pore size is indicated on the graph.

Figure 8: Deconvoluted contributions of macropores from global thermogram for samples A, B and C with calculated mean macropore size.

Figure 9: Values of pore radii of reference silica gels (-□-), and hybrid samples A, B, C for mesopores (-○-) and macropores (-△-) measured by nitrogen gas sorption and mercury porosimetry respectively. Dotted line represents the values predicted by the use of Equation (3) while solid line is the best ODR fit to experimental results.

Table 1: Textural data of samples A, B and C. Specific surface area ( $S_{\text{spec}}$ ) and mean mesopore radius ( $r_{\text{meso}}$ ) measured by nitrogen gas sorption and macropore radius ( $r_{\text{macro}}$ ) measured by mercury porosimetry.

Table 2: Comparison of pore radii measured by TPM with data obtained for mesopores and macropores by gas sorption and mercury porosimetry respectively.

Sample	C(HCl) (mol/l)	N <sub>2</sub> -Sorption measurement		Mercury porosimetry
		S <sub>spec</sub> (m <sup>2</sup> /g)	r <sub>meso</sub> (nm)	r <sub>macro</sub> (μm)
A	1	838	3.1	0.140
B	0.1	981	2.9	0.240
C	0.03	942	2.9	0.190

Table 1

sample	r <sub>meso</sub> (N <sub>2</sub> ) (nm)	r <sub>meso</sub> (TPM) (nm)	V <sub>meso</sub> (N <sub>2</sub> ) (cm <sup>3</sup> .g <sup>-1</sup> )	V <sub>meso</sub> (TPM) (cm <sup>3</sup> .g <sup>-1</sup> )	r <sub>macro</sub> (Hg) (μm)	r <sub>macro</sub> (TPM) (μm)
A	3.1	3.2	0.9	0.92	0.140	0.162
B	2.9	2.9	0.99	1.02	0.220	0.245
C	2.9	2.8	1.42	1.50	0.190	0.184

Table 2





Figure 1

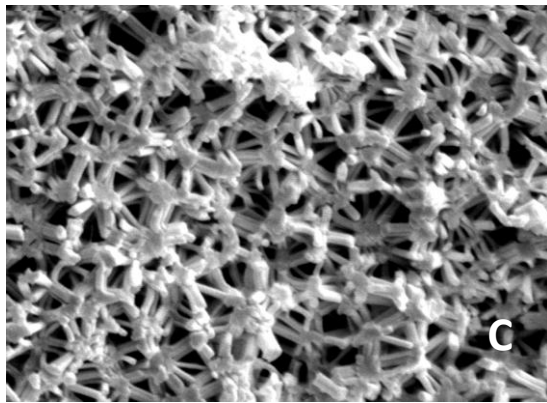
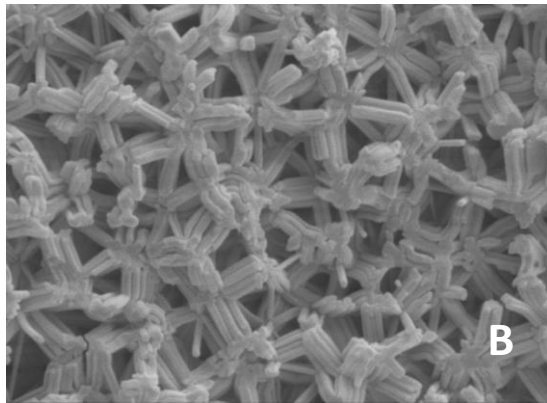
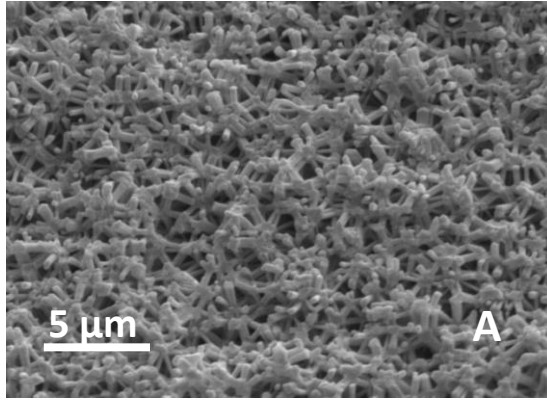


Figure 2

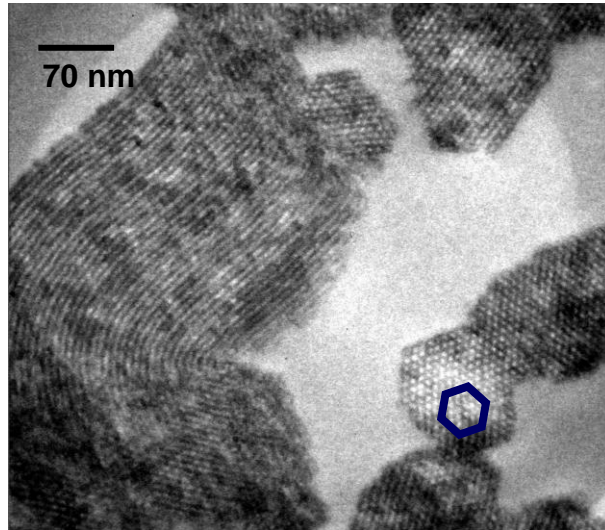


Figure 3

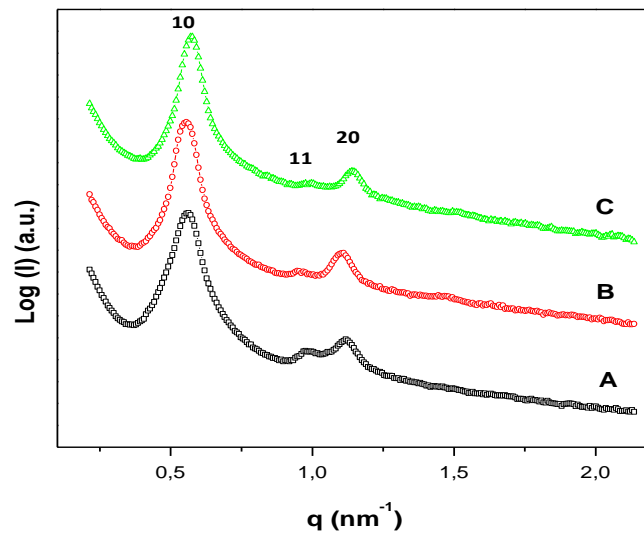


Figure 4

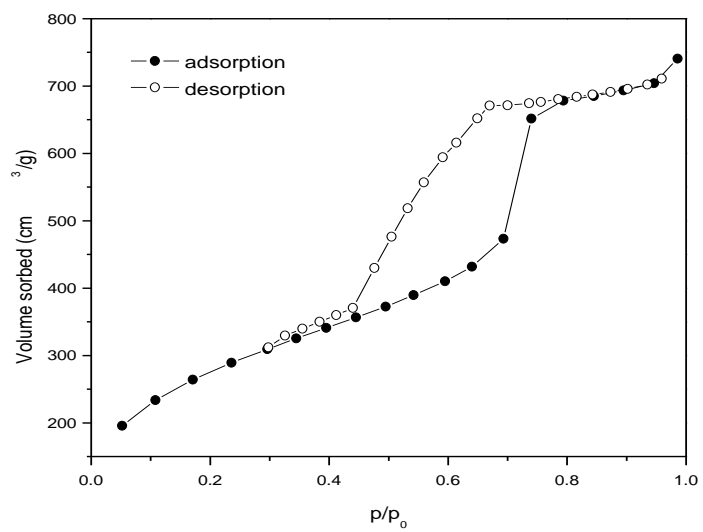


Figure 5

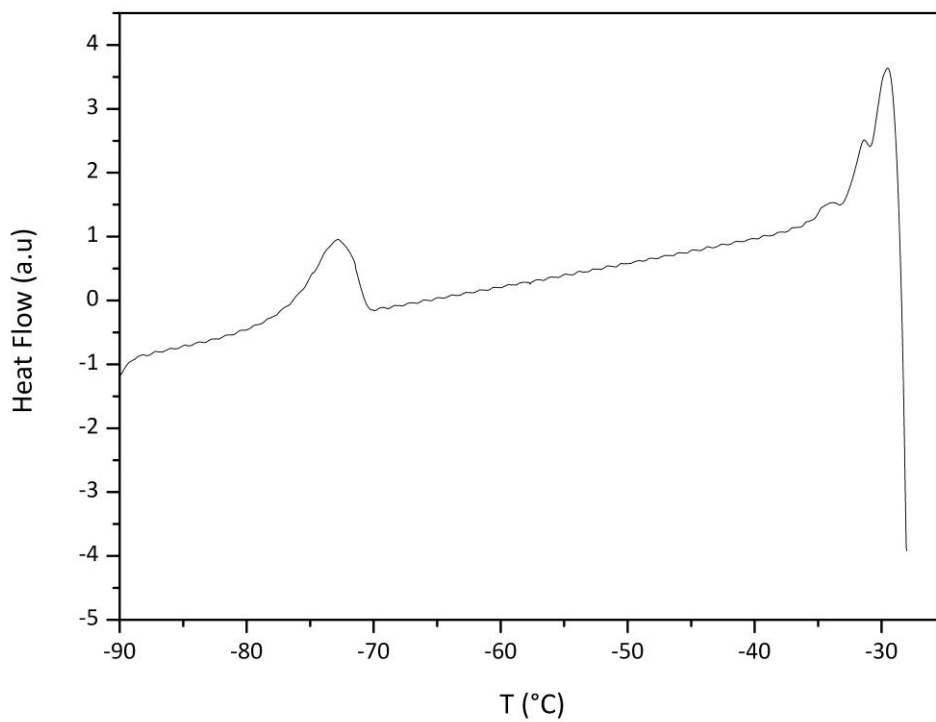


Figure 6

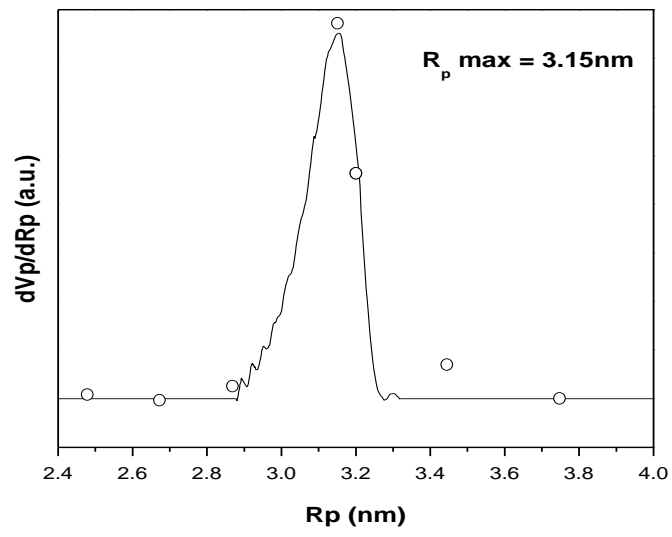


Figure 7

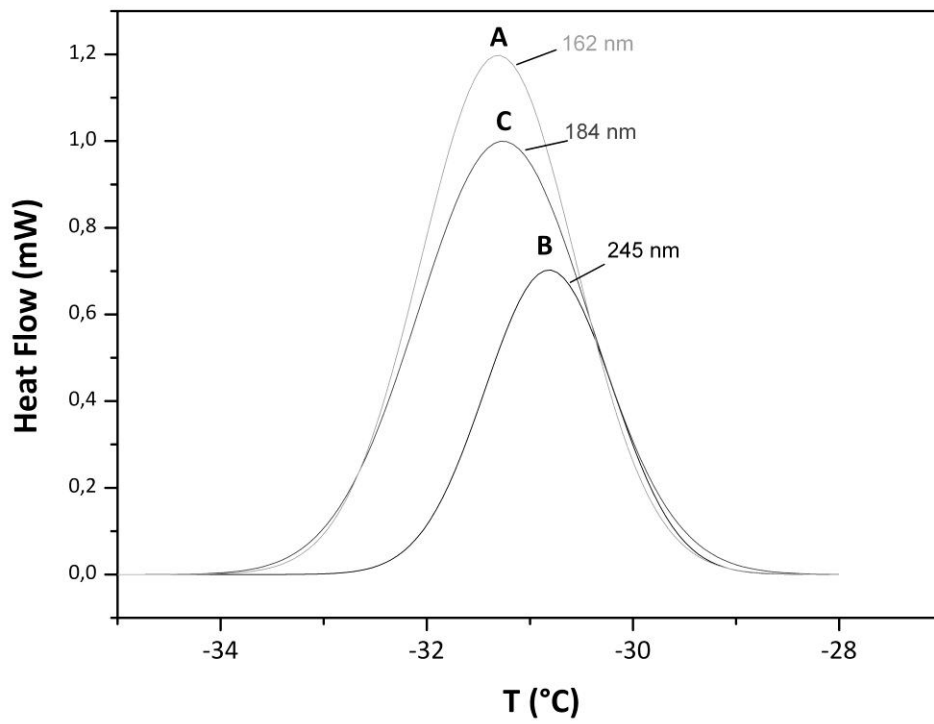


Figure 8

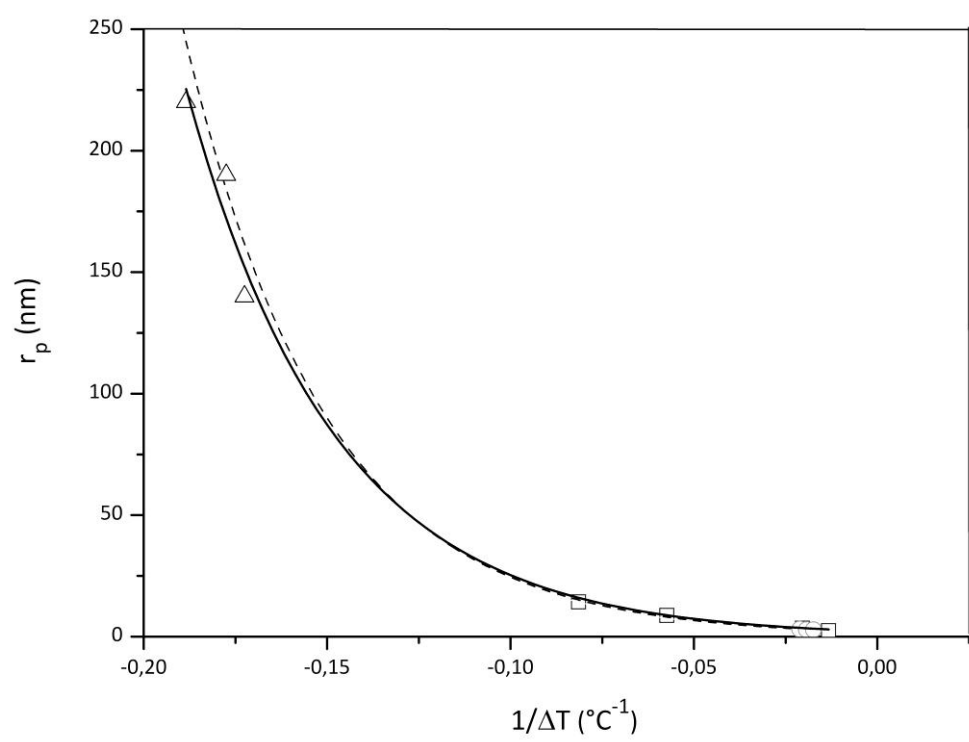


Figure 9

## References

---

- [1] Sanchez C., Arribart H. and Giraud Guille M.-M. *Nature Materials*, **2005**, *4*, 277.
- [2] Mann S., Ozin G. A. *Nature*, **1996**, *382*, 313.
- [3] Keppeler M., Hüsing N. *New J. Chem.* **2011**, *35(3)*, 681.
- [4] El Kadib A., Chimenton R., Sachse A., Fajula F., Galarneau A., Coq B *Angew. Chem. Int. Ed.*, **2009**, *121*, 5069.
- [5] Sachse A., Fajula F., Galarneau A., Fajula F., F. Di Renzo, Creux P., Coq B *Micropor. Mesopor. Mater.*, **2011**, *140(1-3)*, 58.
- [6] Nunez O., Nakanishi K., Tanaka N. *J. Chromatogr. A*, **2008**, *1191(1-2)*, 231.
- [7] Altmaier S., Cabrera K. *J. Sep. Sci.* **2008**, *31(14)*, 2551.
- [8] Nakanishi, K., Tanaka N. *Acc. Chem. Res.* **2007**, *40*, 863-873.
- [9] Hartmann S., Brandhuber D., Hüsing N. *Acc. Chem. Res.* **2007**, *40*, 885-894.
- [10] Cha J.N., Stucky G.D. , Morse D.E., Deming T.J. *Nature* **2000**, *403*, 289
- [11] Yang P.D., Deng T., Zhao D.Y., Feng P.Y., Pine D., Chmelka B.F., Whitesides G.M., Stucky G.D., *Science* **1998**, *282*, 2244.
- [12] Lin H.P. , Mou C.Y. *Science* **1996**, *273*, 765.
- [13] Gibbs J. *Collected works, New Haven, CT : Yale University Press* **1928**.
- [14] Thomson S.W. *Phil. Mag.* **1871**, *42*, 448.
- [15] Jackson C.L., McKenna G.B. *J. Chem. Phys.* **1990**, *93(12)*, 9002.
- [16] Kunh W., Peterli E. and Majer H. *J. Polymer Sci.* **1955**, *16*, 539.
- [17] Fagerlund G. *Matériaux et constructions* **1973**, *6(33)*, 215.
- [18] Brun M., Lallemand A., Quinson J.-F. and Eyraud C. *Thermochim. Acta* **1977**, *21*, 59.
- [19] Gane P., Ridgway C., Lehtinen E., Valiullin R., Furo I., Schoelkopf J., Paulapuro H. and Daicic J. *Ind. Eng. Chem. Res.* **2004**, *43*, 7920.
- [20] Baba M., Nedelec J.M., Lacoste J. *J. Phys. Chem. B*, **2003**, *107*, 12884.
- [21] Nedelec J.M., Grolier J.-P.E. and Baba M. *J. Sol-Gel Sci. Technology*, **2006**, *40*, 191.
- [22] Nedelec J.M., Grolier J.-P.E., Baba M. *Phys. Chem. Chem. Phys.*, **2008**, *10*, 5099.
- [23] Baba M., Nedelec J.M., Lacoste J., Gardette J.-L. and Morel M., *Polymer Degrad. Stabil.* **2003**, *80(2)*, 305.

- 
- [24] Elimelech H., Nedelec J.M., Hardy-Dessources A., Babonneau F. and Avnir D. *J. Mater. Chem.*, **2010**, *20*, 9515.
- [25] Seisenbaeva G.A., Moloney M.P., Tekoriute R., Hardy-Dessources A., Nedelec J.M., Gun'ko Y.K. and Kessler V.G. *Langmuir*, **2010**, *26(12)*, 9809.
- [26] Wulff M. *Thermochim. Acta*, **2004**, *419*, 291.
- [27] Takei T., Ooda Y., Fuji M., Watanabe T. and Chikazawa M. *Thermochim. Acta*, **2000**, *352-353*, 199.
- [28] Mehrotra R.C. and Narain R.P. *Indian J. Chem.*, **1966**, *5*, 444.
- [29] Brandhuber D., Torma V., Raab C., Peterlik H., Kulak A., Hüsing N. *Chem. Mater.*, **2005**, *17*, 4262.
- [30] Huesing N., Raab C.K., Torma V., Peterlik H. *J. Mater. Chem.*, **2005**, *15*, 1801.
- [31] Braun S., Kalinowski H.-O., Berger S., *150 and More Basic NMR Experiments, Wiley-VCH Verlag Weinheim, 2nd expanded edition 1998*, 322.
- [32] Wagner R., Berger S., *Phosphorus, Sulfur, and Silicon 1994*, *91*, 213.
- [33] F. Rouquerol, J. Rouquerol, K. S. W. Sing, in Handbook of Porous Solids, Vol. 1 (Eds.: F. Schüth, K. S. W. Sing, J. Weitkamp), Wiley-VCH, Weinheim, **2002**, pp. 236.
- [34] E. P. Barrett, L. G. Joyner, P. P. Halenda, *J. Am. Chem.Soc.* **1951**, *73*, 373.
- [35] D.-Y. Zhao, J. Feng, Q. Huo, N. Melosh, G. H. Fredrickson, B. F. Chmelka, G. D. Stucky, *Science*, **1998**, *279(5350)*, 548.
- [36] D. Brandhuber, N. Hüsing, H. Peterlik, *J. Mater. Chem.*, **2005**, *15*, 3896-3902.
- [37] M. Keppeler, J. Holzbock, J. Akbarzahdeh, H. Peterlik, N. Hüsing, *Beilstein J. Nanotechnol.* **2011**, *2*, 486-498.
- [38] Billamboz N., Baba M., Grivet M. and Nedelec J.M. *J. Phys. Chem B*, **2004**, *108(32)*, 12032.
- [39] Billamboz N., Nedelec J.M., Grivet M. and Baba M. *ChemPhysChem* **2005**, *6(6)*, 1126.
- [38] Valot P., Sintès-Zydowicz N., Nedelec J.-M., Baba M. *J. Polym. Sci. B* **2010**, *48(18)*, 1939.